Efficient Liver Segmentation using Advanced 3D-DCNN Algorithm on CT Images

S. Subha
Department of Computer Applications, Noorul Islam Centre for Higher Education, Thuckalay, Kanyakumari, India
subhasundar93@gmail.com (corresponding author)

U. Kumaran
Department of Computer Applications, Noorul Islam Centre for Higher Education, Thuckalay, Kanyakumari, India
kumaran.u@rediffmail.com

Received: 2 October 2024 | Revised: 5 November 2024 | Accepted: 20 November 2024

 DOI: https://doi.org/10.48084/etasr.9157

ABSTRACT

According to the latest global cancer statistics for 2022, liver cancer ranks as the ninth most common disease in women. Segmenting the liver and distinguishing it from tumors within it pose a significant challenge due to the complex nature of liver imaging. Common imaging methods such as Magnetic Resonance Imaging (MRI), Computer Tomography (CT), and Ultrasound (US) are employed to distinguish liver tissue from liver tumors after collecting a sample. Attempting to partition the liver and tumor based on grayscale shades or shapes in abdominal CT images is not ideal because of the overlapping intensity levels and the variability in the location and shape of soft tissues. To address this issue, this study introduces an effective method for liver image segmentation using a 3D deep Convolutional Neural Network (3D-DCNN). The process involves several stages. First, liver images undergo preprocessing to enhance image quality, including median filtering, adaptive filtering, and converting them to grayscale. The feature extraction phase focuses on extracting four sets of features, such as the Local Binary Pattern (LBP) and the Gray-Level Co-occurrence Matrix (GLCM). Additionally, an Iterative Region Growing (IRG) technique is developed to improve the Dice Similarity Coefficient (DSC) prediction by enhancing the quality of the input images obtained from segmented images. This method enables the segmentation of the liver in abdominal CT image volumes and can subsequently be used to segment liver tumor images to evaluate the performance of the proposed 3D-DLNN approach. This method was implemented in MATLAB, and its performance was evaluated using various metrics. In experimental analysis, the proposed technique outperformed other methods, including Jaccard with JISTS-FCM, Fuzzy C-Means (FCM), and FCM with Cluster Size Adjustment (FCM-CSA).

Keywords-Iterative Region Growing (IRG) algorithm; liver segmentation; feature extraction; CT image, 3D deep convolutional neural network

I. INTRODUCTION

The liver provides essential functions for both animals and vertebrates. Liver diseases in humans can be life-threatening, often without prior warning. Therefore, the early diagnosis of liver conditions is crucial [1, 2]. Liver tumors are a prevalent type of internal cancer and are associated with high mortality rates. Liver cancer is ranked as the tenth most common cancer and ranks as the fifth and ninth leading causes of cancer-related deaths in men and women, respectively. Early detection of cancer significantly improves survival rates for most cancer types [3, 4]. Computed Tomography (CT) is a key and highly effective imaging method for detecting liver cancers. CT scans provide images of the entire liver through sequential scans after the injection of a contrast agent. Manual segmentation of CT scans is a challenging and time-consuming process that can delay clinical procedures [5].

Segmentation is a critical and indispensable process in image processing, and it is one of the most challenging tasks [6, 7]. Automating tumor segmentation in liver CT images presents significant difficulties due to various factors, including low image contrast, fuzzy edges, variations in liver shape and size between patients, and similarities in intensity with adjacent organs such as the spleen and stomach [8]. Furthermore, automated segmentation of the liver and lesions poses challenges because the liver parenchyma can span across 150 slices in a CT image, making it distinct for each patient. Lesions often exhibit poorly defined shapes and poor intensity contrast relative to surrounding tissue and similarities with neighboring structures. Traditional image segmentation

algorithms have limitations that hinder their ability to achieve precise results efficiently [9].

Manual segmentation and classification of liver lesions from CT images, especially for lesions such as hemangioma and metastasis that closely resemble the liver in appearance, is a time-consuming task, and the results obtained tend to be less reliable. Therefore, there is an urgent need for the development of automated methods to assist radiologists in identifying liver lesions from CT scans. Traditionally, automated liver analysis involves several key steps, including lesion detection, liver segmentation, lesion classification, and follow-up. The proper categorization of medical images heavily relies on deep learning models such as Convolutional Neural Networks (CNNs).To address various challenges in medical image analysis, researchers have turned to bio-inspired meta-heuristic optimization algorithms, such as Social Spider Optimization (SSO), Ant Colony Optimization (ACO), Crow Search Optimization (CSO), and Particle Swarm Optimization (PSO). These computational bio-inspired algorithms are employed when conventional methods fall short or prove to be time-consuming. This work presents a highly effective optimization strategy, focusing on both speed and optimal convergence, to address a wide range of segmentation issues in medical images.

Various techniques and studies have been proposed to address image segmentation challenges in general and, more specifically, in the field of medical imaging. In [10] a CNN was proposed for automated liver segmentation. This study initially employed a fractional differential enhancement approach for preprocessing. Subsequently, a CNN was used to perform the initial liver segmentation, followed by the development of an active contour model for precise liver segmentation. Experimental results showed that this approach outperformed previous methods. In [9], an automated liver segmentation method was proposed for CT scans. A squeeze-and-excitation block was introduced along with an atrous spatial pyramid pooling based on the U-Net architecture. The squeeze-and-excitation block emphasized important features while suppressing unnecessary areas. The atrous spatial pyramid pooling collected multiscale image data with various receptive fields. This study also replaced standard convolution blocks with residual structures to address gradient vanishing issues, enabling the network to achieve greater depth and accuracy.

In [11], a cascaded deep Encoder-Decoder CNN (EDCNN) was developed for effective liver tumor segmentation. EDCNN was trained to cascade segments of the liver and lesions in CT scans, where one EDCNN divided the hepatic image into segments as training input for another. This approach significantly reduced false positive results when segmenting liver Regions Of Interest (ROIs) that included hepatic tumors. In [12], a liver segmentation method on abdominal CT volumes was developed, based on level sets and sparse form composition. A Sparse Shape Composition (SSC)-based technique was also introduced to enhance segmentation results for damaged livers by refining liver shapes. This level-set-based approach addressed intensity inhomogeneity in object areas, while the SSC- and graph-cut-based approach effectively handled under-segmentation issues seen in diseased livers. In [13], a global context and hybrid attention network was introduced for automated liver segmentation. This study designed a Global Attention Module (GAM) to capture interdependencies in channel and positional dimensions, representing global characteristics. A Local Attention Module (LAM) was used to gather spatial information and a Feature Aggregation Module (FAM) was introduced to focus on local hepatic areas. This model effectively reduced irrelevant data and increased focus on relevant liver regions.

II. PROPOSED EFFICIENT LIVER SEGMENTATION METHOD

A. Dataset Description

The training set from the LiTS Liver Tumor Segmentation Challenge was used to evaluate the proposed technique. This dataset comprises 131 contrast-enhanced CT scans obtained from various hospitals around the world. The 3DIRCADb dataset is a subset of the LiTS dataset, encompassing cases numbered from 27 to 48. The 3DIRCADb dataset [14] was used for evaluation. Within the training dataset, 100 labeled slices and 900 unlabeled slices were selected from different participants. This selection aimed to enable the validation of the proposed method's performance in a scenario with limited labeled data.

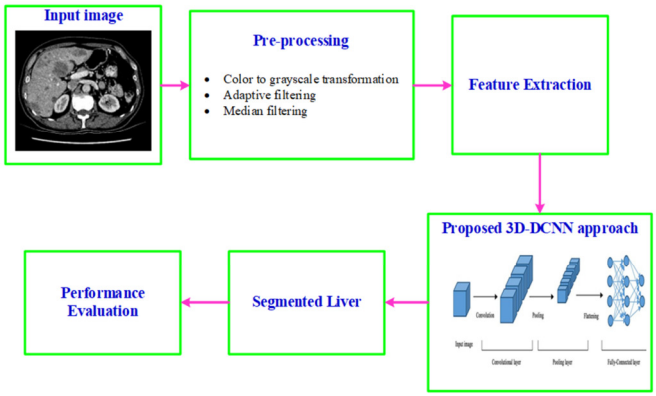

Fig. 1. Block diagram of the proposed method.

B. Method

Currently, radiologists manually segregate liver tumors on several CT scans using slice-by-slice analysis. The manual method is time-consuming and difficult. For computer-assisted diagnosis, segmented areas are offered, while manually segmented images can lead to less effective diagnosis. Automatic liver and liver tumor segmentation models face several challenges, including (a) low brightness of the CT images in the liver tumor and healthy tissue and blurring of the boundaries around the liver tumor, (b) the size, location, and shape of liver tumors vary, and (c) the liver is closely connected to adjacent organs, which will have CT values similar to the liver. Figure 1 shows the architecture of the proposed liver tumor segmentation approach.

C. Data Preprocessing

The preprocessing stage involved methods such as median filtering, adaptive filtering, and color-to-grayscale conversion. The collected images were first pre-processed to change them into the necessary image format [15]. The primary goal of the preprocessing stage is to sharpen crucial aspects for subsequent processing while reducing unimportant distractions from the liver tumor image features.

1) Color to Grayscale Transformation

The color-to-grayscale conversion improves the image quality, increasing model speed and scalability.

2) Adaptive Filtering

The adaptive filters are used as a denoiser during image processing to reduce noise without degrading the image quality. The orientation-controlled adaptive filter can be represented as:

$$\Psi_{AF} = \Psi_{AF}(\varphi, P) \quad (1)$$

where P stands for the anisotropy and φ denotes the orientation parameter. Using orientation evaluation as the initial parameter, the noise in the source image can be reduced.

3) Median Filtering

It is inevitable to keep an image's spatial properties after using the de-noising technique. Therefore, to prevent the image borders from becoming blurry, a non-linear smoothing filter, known as the median filter, was used [16]. Utilizing a median filter may assist in replacing a needed point with brightness obtained from its nearby edge. This happens because the sounds have no impact on the median brightness of the neighboring edge. The impulse noise is also eliminated by the median filter. Using the median filter results in a better-quality image of the ultrasound liver tumor image. The output is represented as:

$$MF_P(r,s) = med\{P(r-x, s-y)x, y \in M\} \quad (2)$$

where MF_P and P denote the median filtered and the original images, respectively, and med is the median filtering method that uses a 2D mask. To facilitate additional processing, segmentation is applied to the final output.

D. Feature Extraction

After segmentation comes a feature extraction process, which is one of the most important image processing techniques to redefine large redundant data into small features. From the segmented image, the amount of exudate, the separation between the shape of the liver tumors, LBP, and the Grayscale Compatibility Matrix (GLCM) properties are extracted. The classification ability is tested through extensive computer simulations to find the most unique identifiers that complement the best recognition performance.

Characteristics of the liver tumor, color, GLCM, and form are extracted. According to the liver tumor and the healthy tissue, the properties of the CT image are a more crucial characteristic for discrimination [17]. The CT image shape analysis method extracts the boundary and region-based characteristics. A probability distribution is described by a second-order statistic that involves the probability that two pixels with a given gray level appear in some spatial relationship. These data, calculated using various orientations and separations, are displayed in two-dimensional gray-level display matrices.

In addition to the above-described elements, the following liver tumor vessel-based features were employed. The energy of the cells, called the volume unit, is an important factor in laboratory imaging. Feature Δ is defined as:

$$\Delta = \sum_x \sum_y \eta^2(x,y) + \left(\sqrt{-1}\right) * \left(\frac{\sqrt{\sum_{x=1}^{z} (w_x - w')^2}}{z-1} \right) \quad (3)$$

Thus, the normalized GLCM element for the x^{th} row and the y^{th} column is represented as $w' = \sum_{x=1}^{y} \frac{w_x}{z}, \eta(x,y)$.

1) Local Binary Pattern (LBP)

LBP is a reliable and effective texture descriptor that might be used in a variety of applications, from liver tumors to texture segmentation. The LBP operator categorizes the image pixels by thresholding the area around each pixel with the center value, and this thresholding output is taken as the binary value [18]. After each pixel is classified according to the LBP codes, a label histogram $LI_{ABN}(i,j)$ is calculated and used as a description of the texture. If k is true, $L(k) = 1$, and if K is false $L(k) = 0$. The number of unique labels returned by the LBP operator and the histogram of the labeled image are used as a description and comparison using:

$$\Delta_{HS}(Pic) = \sum_{i,j} L(LI_{ABN}(x,y) = Img)$$
$$Img = 0, \ldots\ldots, k-1 \quad (4)$$

Additionally, a pixel's neighborhood is captured in a circle. λ points with radius γ are chosen throughout the circle's perimeter. Using (5), the uniformity metric (Δ_{UM}) is calculated by utilizing $\Delta_{LBP}(\lambda, \gamma)$, a λ -bit binary value $(i_{\lambda-1}, i_{\lambda-2}, \ldots, i_1, i_0)$ to provide a uniform pattern that is rotation-invariant with finer angular quantization.

$$\Delta_{UM}\left(\Delta_{LBP}(\lambda,\gamma)\right) = |i_{\lambda-1} - i_0| + \sum_{\alpha=1}^{\alpha-1} |i_\lambda - i_{\lambda-1}| \quad (5)$$

cp_{GV} denotes the gray value of the center pixel, λ denotes the gray values of the points, and $\lambda = 0, \ldots, \lambda - 1$. In (5), a value less than or equal to 2 gives a homogeneous pattern Δ_{UM} rotation model. A multiscale assessment is carried out using LBP by choosing circles of different radii around the center pixels and producing a different LBP image for each size. Additionally, the LBP image's energy and entropy, $S = 1, 2, 3$, which are constructed from several different pixel counts $\lambda = 8, 16, 24$, are used as feature descriptors.

$$\Delta_{LBP}(\lambda, S) = \begin{cases} \sum_{\alpha=0}^{\alpha-1} S(cp_{GV}(\lambda) - cp_{GV}) \; if \Delta_{UM}\left(\Delta_{LBP}(\lambda,S)\right) \leq 2 \\ \lambda + 1 \qquad\qquad otherwise \end{cases} \quad (6)$$

2) Segmentation using Iterative Region Growing Algorithm-based 3D DCNN

The final image uses the 3D-DCNN-based optimum region growth approach to separate the tumor from the liver portion.

This is a single-seeded region-expanding algorithm in its modified form. The seeded region growth concept is used for different types of tumor segmentation. The 3D-DCNN model is created for tumor and liver semantic segmentation based on the effectiveness of deep learning models in medical image segmentation [19]. This section provides a detailed explanation of 3D-DCNN.

The 3D-DCNN is one of the most advanced deep learning techniques and is a feedforward neural network with a joining architecture for its neurons. In brain tumor semantic segmentation, overlapping districts of various neurons are formed from neurons. The 3D-DCNN was created using a sophisticated architecture of stacked layers and is a very robust and sensitive architecture for identifying every feature in the image. Figure 2 outlines the 3D DCNN's fundamental structure.

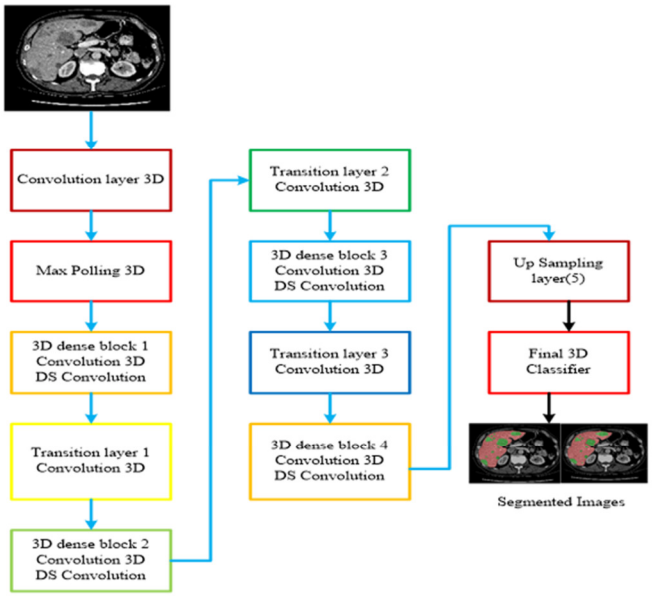

Fig. 2. Architecture of the 3D-DCNN model.

In this study, a 3D-DCNN was created and utilized to segment the liver tumors. The DCNN consists of the output, fully connected, flattened, three-dimensional input, and two convolutional layers. The first layer is the 3D input layer. The second layer is a 3D convolutional layer made up of a 3D Batches Normalization (BN) layer, a Rectified Linear Unit (ReLu), and a 3D convolution layer. To extract the features, the 3D convolution layer has a filter size that advances along the time axis. The third layer is a 3D convolution layer, which includes a batch normalizing layer, a convolution layer, and a 3D ReLu layer. By shifting the horizontal axis, the third layer of the 3D model is used to extract time-domain characteristics. The fourth layer, which consists of a C3 vector array, is referred to as a 3D flattened layer [20]. The 3D fully linked layer follows. The final 3D Softmax is used to separate the liver tumor from the CT image. In 3D-DCNN, a neuron is described as:

$$Ne(E,F,G) \tag{7}$$

where G denotes several position feature maps, F denotes several feature maps, and E denotes several layers of a neural network. The neuron's input and output may be expressed as $I_E^F(G)$ and $Z_E^F(G)$. The following formulas can be used to express the relationship between input and output:

$$Z_E^F(G) = F(A) = F\left(Z_E^F(G)\right) \tag{8}$$

The activation function, F, is written as follows:

$$F(A) = ln(1 + e^{\alpha}) \tag{9}$$

The symbol for the input image is:

$$I_{E1}^F(G)(Ne_C@Ne_{FR} * Ne_T) \tag{10}$$

The output expression for the second convolution layer is:

$$Z_F^2(G) = F(A) = F(\sum_{E=1}^{n} I_{E1}^F * f_F^2 + B_F^2(G))$$
$$F = 1,2,3,\ldots.n \tag{11}$$

where B_F^2 is characterized as a bias, f_F^2 describes a filter, and $Z_F^2(G)$ is the output layer of C_3. The feature vector and this filter slide together horizontally to produce the vectors. Before transferring the input from the activation layer, these vectors may be regularized with the aid of the BN layer. The input of layer 4 is then merged to create a vector. Layer 5 has a completely linked layer as its last component, and its output is described by the following mathematical formulation:

$$Z_5 = F(A) = F\left(\sum_{E=1}^{n} Z^4 * f_E^5 + B^5\,(G)\right) \tag{12}$$

where f_E^5 can be interpreted as fifth-layer weights and B^5 can be seen as fifth-layer biases. The softmax layer, which includes the two neurons, is the sixth layer. The mathematical formulation for the sixth layer output is as follows:

$$Z_6 = F\left(\sum_{E=1}^{n} Z^5(E) * f^6(E) + B^6\,(F)\right) \tag{13}$$

The 3D DCNN network's forward propagation computation flow is derived from the aforementioned equations. The biases and weights of the 3D DCNN network take the error backpropagation technique into account. The labeled training dataset is used to train the 3D DCNN network. Gradient descent is used to update the weights and biases in a 3D DCNN as follows:

$$f^G = f^G - \omega \frac{\partial E}{\partial f^G} \tag{14}$$

$$B^G = B^G - \omega \frac{\partial E}{\partial B^G} \tag{15}$$

The 3D DCNN's training step involves computing and resolving the minimal error rate. This 3D DCNN structure does not have a pooling layer. The DCNN network omits the pooling layer, abbreviates the network architecture, and avoids inappropriate optimum features. Each feature vector may be standardized by sending the feature vectors to the ReLU layer as input. Layer 4 joins the time domain and frequency feature vectors, which were previously sent to the fully linked layer [21]. Finally, the segmentation phase might take into account the Softmax layer. Here, the ground-truth label and training samples for the input image are shown as follows:

$$In \in \gamma^{n(224*224*12)*CH} \tag{16}$$

$$Out \in \gamma^{n(224*224*12)*1} \quad (17)$$

In this case, the input batch size n and the channel CH can be defined.

3) Iterative Region Growing Algorithm

A region is an independent geographic grouping of pixels that is represented by a node in a Region-Growing Adjacency Graph (RGAG), and a link is the shared border between two regions. The segmentation and classification algorithms leverage the edge strength between each pair of neighboring regions [22]. In (18), it is shown that it is feasible to penalize weak edges more severely than strong edges instead of equally for all boundary-site pairings.

$$\alpha(\nabla_{st}) = \alpha(|z_s - z_t|) = e^{-\left(\frac{|z_s - z_t|}{D}\right)^2} \quad (18)$$

where γ is a positive integer and s and t are the nearby spots that form a pair-location clique. Each pixel's gray level is constant z_s and tied to its matching class name z_t. The IRG technique approaches the segmentation formulation of (19) from the common Gaussian mixture issue using a series of objective functions (with D increasing):

$$F = arg \min_{\{\omega, s\in S\}} \left\{ \sum_{s\in S} \left(\frac{1}{2} ln\left(2\pi\tau_{n_s}^2\right) + \frac{\left(z_s - \mu_{n_s}\right)^2}{2\mu_{\omega_s}^2} \right) + \gamma \sum_{\langle s,t\rangle \in Z} \left[\left(1 - \beta(z_s - z_t)\right) \omega(\nabla_{st}) \right] \right\} \quad (19)$$

Iterative segmentation is used in the IRG procedure. At each iteration, a region-merging technique is used to solve the objective function (19) for a particular D, with region-based labeling [23] serving as the merging criterion.

$$\beta E = \sum_{s\in\omega_x} ln(\omega_x) - \sum_{s\in\omega_y} ln(\omega_y) - \sum_{s\in\omega_z} ln(\omega_z) - \gamma \sum_{\substack{s\in\partial\omega \\ t\in\partial\omega_z, t\in\delta_s}} \omega(|z_t - z_s|) \quad (20)$$

where ω_x and ω_y are the names of the two regions, $\omega_z = \omega_x \cup \omega_y$ and $\partial\omega_x$ is the collection of border locations of η_x (i.e. $\exists t \in \delta_s, m_s \neq m_t$). If βE generates an undesirable value, ω_x and ω_y can be added together. If βE produces a positive value, ω_x and ω_y cannot be added together. After the region-merging process is complete (i.e., no more region pairs satisfy the merging requirement), an RGAG may be updated using the recovered regions. Using an edge stop function based on the RGAG, the region-based labeling procedure and the associated single-node clique-energy function can be mimicked.

$$\Delta_1(m_x) = \sum_{s\in\omega_t} \left\{ \frac{1}{2} ln\left(2\pi\mu_{z_t}^2\right) + \frac{\left(c_s - \tau_{z_t}\right)^2}{2\mu_{z_t}^2} \right\} \quad (21)$$

as well as the pair-node clique energy being:

$$\Delta_2(m_x, m_y) = \begin{cases} \gamma \sum_{\substack{s\in\partial\omega \\ t\in\partial\omega_z, t\in\delta_s}} \omega(|c_t - c_s|), if z_x \neq z_y \\ 0 \end{cases} \quad (22)$$

where τ_{m_t} and $\mu_{m_t}^2$ denote the mean and variance of all the pixel values in the class, and the label of the area is m_s and m_i. The global minimum of the sum of the aforementioned energies throughout the whole RGAG, which is exactly given in (18), can be used to produce a label for the current iteration.

III. PERFORMANCE EVALUATION

The effectiveness of the proposed approach was evaluated through performance and comparative analysis. The evaluation of the proposed CT image semantic segmentation was carried out on a laptop equipped with an Intel Core i5-2450M CPU and 6 GB of RAM using MATLAB R2022b. The proposed strategy was trained and validated using metrics such as the Dice Similarity Coefficient (DSC) and accuracy. Specifically, the proposed 3D-DCNN approach was applied to segment liver tumors in the images. Figures 3 and 4 show the comparative results of the proposed and other methods. The 3Dircadb01 dataset in this instance had 20 CT images. The average findings of 10 CT images randomly chosen from the dataset were used for the testing. On the 3Dircadb01 dataset, the proposed model achieved 98.6% DSC, 94.23% JSC, 99.51% accuracy, 98.6% precision, 97.45% sensitivity, and 98.56% sensitivity. These results show that the proposed method outperformed previous approaches such as JISTS-FCM, FCM-CSA, and FCM.

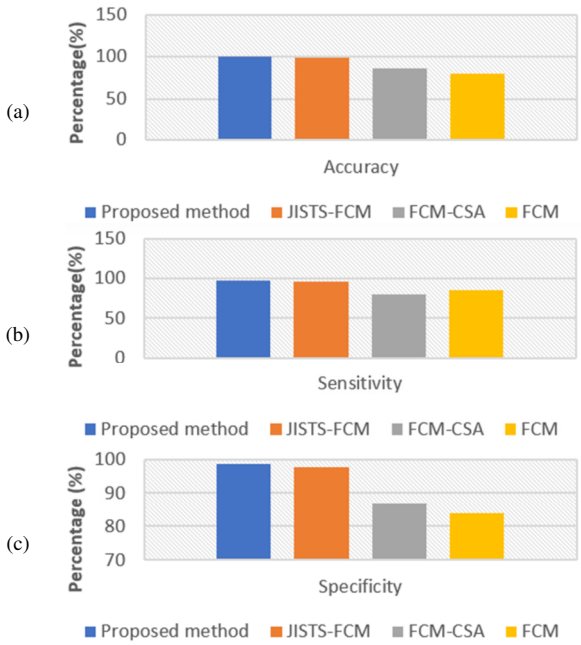

Fig. 3. Proposed method's (a) Accuracy, (b) Sensitivity, and (c) Specificity, on the 3DIRCADb dataset.

A tiny dataset was used for testing and the segmentation results were encouraging. Table I shows the comparative results of the proposed with other methods. The proposed approach produced encouraging segmentation results on liver segmentation when compared to previous methods. Both semi-automatic approaches in [23, 24] require the user to choose the seed spots. The proposed technique performed better than these methods, as it achieved a DSC of 98.12%. On the same dataset, CNN-LivSeg [25] achieved a DSC of 95.41%. The proposed method was also superior to Random Walker (94.03%), Graph-Based Random Walker (93.00%), DBN-DNN [26] (91.83), and JISTS-FCM (97.55%).

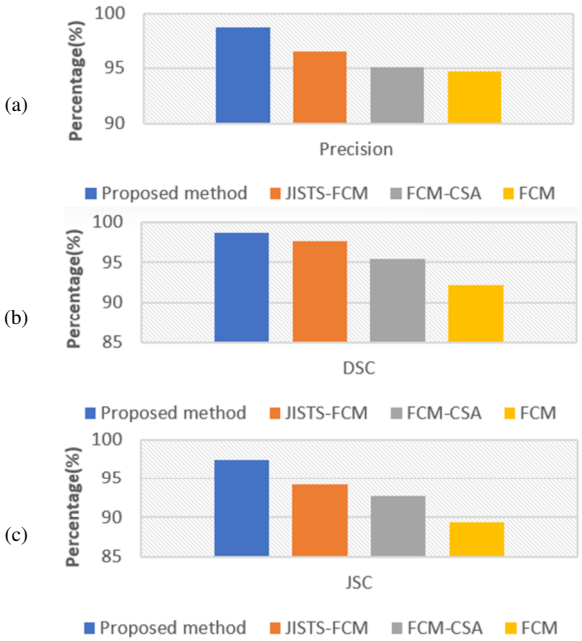

Fig. 4. Proposed method's (a) Precision, (b) DSC, and (c) JSC in 3DIRCADb dataset.

TABLE I. COMPARISON WITH OTHER METHODS

Method	Test dataset (s)	DSC (%)
Random Walker [23]	SLiver'07	94.03
Graph-based Random Walker [24]	LiTS17	93.00
CNN [25]	LiTS17	95.41
DBN-DNN [26]	3Dircadb01	91.83
JISTS-FCM	3Dircadb01	97.55
Proposed Method	**3DIRCADb**	**98.12**

IV. CONCLUSION

Preprocessing is a crucial step in improving the input training data used to train deep-learning models that separate the liver from other organs in medical images. The uniqueness of this study is in proposing an approach that is reliable and easily adapted to real-time imaging of liver cancers. This study presented an effective 3D-DCNN method for liver CT image segmentation. The input image is preprocessed by being cropped and adjusting its contrast level using adaptive filtering, median filtering, and color-to-grayscale conversion. The IRG uses a 3D-DCNN to segment images of liver tumors and to identify retinal diseases. For ultimate precision, the features are retrieved and then concatenated to create a feature vector. The proposed approach can be used as a preprocessing strategy for image segmentation and feature extraction because of its improved performance. This approach was put into practice using MATLAB 2022a and compared with previous methods. The 3DIRCADb dataset showed that the proposed technique was successful in segmenting the liver and tumors in heterogeneous CT scans from several scanners, demonstrating its generalizability and making it a viable tool for automated analysis of the liver and associated tumors in clinical practice. When comparing the proposed 3D-DCNN segmentation with current JISTS-FCM, FCM, and FCM-CSA techniques, the proposed approach achieved DSC and accuracy of 0.99 and 0.95, respectively, outperforming them in all metrics examined. This research can be expanded in the future to segment liver lesions and other human organs in medical imaging.

REFERENCES

[1] A. M. Anter and A. E. Hassenian, "CT liver tumor segmentation hybrid approach using neutrosophic sets, fast fuzzy c-means and adaptive watershed algorithm," *Artificial Intelligence in Medicine*, vol. 97, pp. 105–117, Jun. 2019, https://doi.org/10.1016/j.artmed.2018.11.007.

[2] X. Tang *et al.*, "Whole liver segmentation based on deep learning and manual adjustment for clinical use in SIRT," *European Journal of Nuclear Medicine and Molecular Imaging*, vol. 47, no. 12, pp. 2742–2752, Nov. 2020, https://doi.org/10.1007/s00259-020-04800-3.

[3] A. Mostafa, A. E. Hassanien, M. Houseni, and H. Hefny, "Liver segmentation in MRI images based on whale optimization algorithm," *Multimedia Tools and Applications*, vol. 76, no. 23, pp. 24931–24954, Dec. 2017, https://doi.org/10.1007/s11042-017-4638-5.

[4] A. Bereciartua, A. Picon, A. Galdran, and P. Iriondo, "Automatic 3D model-based method for liver segmentation in MRI based on active contours and total variation minimization," *Biomedical Signal Processing and Control*, vol. 20, pp. 71–77, Jul. 2015, https://doi.org/10.1016/j.bspc.2015.04.005.

[5] N. Nanda, P. Kakkar, and S. Nagpal, "Computer-Aided Segmentation of Liver Lesions in CT Scans Using Cascaded Convolutional Neural Networks and Genetically Optimised Classifier," *Arabian Journal for Science and Engineering*, vol. 44, no. 4, pp. 4049–4062, Apr. 2019, https://doi.org/10.1007/s13369-019-03735-8.

[6] G. Li, X. Chen, F. Shi, W. Zhu, J. Tian, and D. Xiang, "Automatic Liver Segmentation Based on Shape Constraints and Deformable Graph Cut in CT Images," *IEEE Transactions on Image Processing*, vol. 24, no. 12, pp. 5315–5329, Sep. 2015, https://doi.org/10.1109/TIP.2015.2481326.

[7] B. Irving *et al.*, "Deep Quantitative Liver Segmentation and Vessel Exclusion to Assist in Liver Assessment," in *Medical Image Understanding and Analysis*, Edinburgh, UK, 2017, pp. 663–673, https://doi.org/10.1007/978-3-319-60964-5_58.

[8] Y. Zhang, Z. He, C. Zhong, Y. Zhang, and Z. Shi, "Fully convolutional neural network with post-processing methods for automatic liver segmentation from CT," in *2017 Chinese Automation Congress (CAC)*, Jinan, China, Oct. 2017, pp. 3864–3869, https://doi.org/10.1109/CAC.2017.8243454.

[9] J. Wang, P. Lv, H. Wang, and C. Shi, "SAR-U-Net: Squeeze-and-excitation block and atrous spatial pyramid pooling based residual U-Net for automatic liver segmentation in Computed Tomography," *Computer Methods and Programs in Biomedicine*, vol. 208, Sep. 2021, Art. no. 106268, https://doi.org/10.1016/j.cmpb.2021.106268.

[10] Z. Gong *et al.*, "A hybrid approach based on deep learning and level set formulation for liver segmentation in CT images," *Journal of Applied Clinical Medical Physics*, vol. 23, no. 1, 2022, Art. no. e13482, https://doi.org/10.1002/acm2.13482.

[11] Ü. Budak, Y. Guo, E. Tanyildizi, and A. Şengür, "Cascaded deep convolutional encoder-decoder neural networks for efficient liver tumor segmentation," *Medical Hypotheses*, vol. 134, Jan. 2020, Art. no. 109431, https://doi.org/10.1016/j.mehy.2019.109431.

[12] J. D. L. Araújo *et al.*, "Liver segmentation from computed tomography images using cascade deep learning," *Computers in Biology and Medicine*, vol. 140, Jan. 2022, Art. no. 105095, https://doi.org/10.1016/j.compbiomed.2021.105095.

[13] H. Liu *et al.*, "GCHA-Net: Global context and hybrid attention network for automatic liver segmentation," *Computers in Biology and Medicine*, vol. 152, Jan. 2023, Art. no. 106352, https://doi.org/10.1016/j.compbiomed.2022.106352.

[14] M. Hussain, N. Saher, and S. Qadri, "Computer Vision Approach for Liver Tumor Classification Using CT Dataset," *Applied Artificial Intelligence*, vol. 36, no. 1, Dec. 2022, Art. no. 2055395, https://doi.org/10.1080/08839514.2022.2055395.

[15] Y. R. Kumar *et al.*, "Statistical Parameter-based Automatic Liver Tumor Segmentation from Abdominal CT Scans: A Potiential Radiomic Signature," *Procedia Computer Science*, vol. 93, pp. 446–452, Jan. 2016, https://doi.org/10.1016/j.procs.2016.07.232.

[16] Y. Kawashima *et al.*, "Using texture analysis of head CT images to differentiate osteoporosis from normal bone density," *European Journal of Radiology*, vol. 116, pp. 212–218, Jul. 2019, https://doi.org/10.1016/j.ejrad.2019.05.009.

[17] A. Das, P. Das, S. S. Panda, and S. Sabut, "Detection of Liver Cancer Using Modified Fuzzy Clustering and Decision Tree Classifier in CT Images," *Pattern Recognition and Image Analysis*, vol. 29, no. 2, pp. 201–211, Apr. 2019, https://doi.org/10.1134/S1054661819020056.

[18] L. Meng, Y. Tian, and S. Bu, "Liver tumor segmentation based on 3D convolutional neural network with dual scale," *Journal of Applied Clinical Medical Physics*, vol. 21, no. 1, pp. 144–157, 2020, https://doi.org/10.1002/acm2.12784.

[19] Z. Deng, Q. Guo, and Z. Zhu, "Dynamic Regulation of Level Set Parameters Using 3D Convolutional Neural Network for Liver Tumor Segmentation," *Journal of Healthcare Engineering*, vol. 2019, no. 1, 2019, Art. no. 4321645, https://doi.org/10.1155/2019/4321645.

[20] G. Wardhana, H. Naghibi, B. Sirmacek, and M. Abayazid, "Toward reliable automatic liver and tumor segmentation using convolutional neural network based on 2.5D models," *International Journal of Computer Assisted Radiology and Surgery*, vol. 16, no. 1, pp. 41–51, Jan. 2021, https://doi.org/10.1007/s11548-020-02292-y.

[21] Z. Yang, Y. Zhao, M. Liao, S. Di, and Y. Zeng, "Semi-automatic liver tumor segmentation with adaptive region growing and graph cuts," *Biomedical Signal Processing and Control*, vol. 68, Jul. 2021, Art. no. 102670, https://doi.org/10.1016/j.bspc.2021.102670.

[22] S. T. Tran, C. H. Cheng, and D. G. Liu, "A Multiple Layer U-Net, Un-Net, for Liver and Liver Tumor Segmentation in CT," *IEEE Access*, vol. 9, pp. 3752–3764, 2021, https://doi.org/10.1109/ACCESS.2020.3047861.

[23] M. Moghbel, S. Mashohor, R. Mahmud, and M. I. B. Saripan, "Automatic liver segmentation on Computed Tomography using random walkers for treatment planning," *EXCLI Journal*, vol. 15, pp. 500–517, Aug. 2016, https://doi.org/10.17179/excli2016-473.

[24] C. Li, A. Li, X. Wang, D. Feng, S. Eberl, and M. Fulham, "A new statistical and Dirichlet integral framework applied to liver segmentation from volumetric CT images," in *2014 13th International Conference on Control Automation Robotics & Vision (ICARCV)*, Singapore, Dec. 2014, pp. 642–647, https://doi.org/10.1109/ICARCV.2014.7064379.

[25] M. Ahmad, Y. Ding, S. F. Qadri, and J. Yang, "Convolutional-neural-network-based feature extraction for liver segmentation from CT images," in *Eleventh International Conference on Digital Image Processing (ICDIP 2019)*, Guangzhou, China, Aug. 2019, Art. no. 159, https://doi.org/10.1117/12.2540175.

[26] M. Ahmad *et al.*, "Deep Belief Network Modeling for Automatic Liver Segmentation," *IEEE Access*, vol. 7, pp. 20585–20595, 2019, https://doi.org/10.1109/ACCESS.2019.2896961.